Scientific paper

Early Age Hardening of Concrete with Heavy Aggregate in Gamma Radiation Source – Impact on the Modulus of Elasticity and Microstructural Features

Mariusz Dąbrowski[1*], Michał A. Glinicki[2], Kinga Dziedzic[3], Daria Jóźwiak-Niedźwiedzka[3], Svyatoslav Sikorin[4], Victor S. Fateev[5] and Eric I. Povalansky[5]

Received 30 January 2021, accepted 6 May 2021 doi:10.3151/jact.19.555

Abstract

The effects of gamma irradiation on concrete properties during early hardening were studied towards radioactive waste storage or accelerated processing at precast plants. Concrete mixtures containing different mineral aggregates (baryte, magnetite, amphibolite) were investigated. During initial 16 hours of hardening the mixes were irradiated using ^{60}Co gamma source at the rate of 3.5 kGy/h. The mechanical properties and microstructural features of irradiated early-age concrete were tested: the secant elastic modulus, the compressive strength, the porosity and pore size distribution. XRD and SEM analysis were also performed. The results indicate both the stiffening and pore refinement in concrete due to early gamma irradiation. Effects of early irradiation on microstructural features of cement matrix were found in the subsurface layer up to the depth of 2 mm. The influence of different mineral aggregates in concrete on the radiation-induced changes of early age properties is discussed.

1. Introduction

Effects of long-term exposure of concrete to ionizing radiation are of primary importance for biological shielding and containment structures in nuclear power plants. They must exhibit stable mechanical properties and high radiation resistance throughout the designed lifetime of structures reaching 60 to 80 years of exposure to severe environmental actions (Rosseel *et al.* 2016; Kurtis *et al.* 2017). A threshold level of absorbed gamma dose of about $2 \cdot 10^8$ Gy was proposed as a limit for defect-free exposure of concrete (Le Pape *et al.* 2016; Pomaro 2016). No consensus on this value has been reached. According to Maruyama *et al.* (2016) such gamma irradiation threshold level has no practical meaning within the practical lifespan of nuclear shielding structures. A smaller absorbed gamma dose could be considered insignificant for the mechanical properties of hardened concrete. However, for early hardening concrete the influence of gamma irradiation can be substantial as it was demonstrated by Mobasher *et al.* (2017), Craeye *et al.* (2009). Early age exposure of concrete to gamma irradiation is of interest for construction of intermediate level radioactive waste storage containments or for accelerated processing of concrete at precast plants. Therefore, it is essential to understand the effects of gamma radiation on early hardening concrete and determine if early irradiation would induce significant changes to the mechanical properties after more than 28 days of curing.

A review of mechanical and physical deterioration of hardened concrete due to prolonged gamma exposure revealed a major role of dehydration of hardened cement paste leading to shrinkage cracking (Maruyama *et al.* 2018). The heat is also generated in the specimens as a result of gamma irradiation (Reches 2019a). Also, the radiolysis of pore water, resulting in H_2 gas as a primary product and H_2O_2 as a secondary product, is considered as the significant phenomenon (Bouniol and Aspart 1998), inducing spalling and micro-cracks in the cement matrix (Mobasher *et al.* 2015). At high doses of gamma radiation an increased formation of calcite was observed (Vodak *et al.* 2011) as a result of reaction of the radiolysis product H_2O_2 with portlandite ($Ca(OH)_2$) to a reaction product that in presence of CO_2 is converted to $CaCO_3$. For slag-blended cements somewhat different effects were observed than for Portland cements. The formation of additional ettringite was observed Richardson *et al.* (1989) in the specimens irradiated to a total dose of 87 MGy over two years at 50°C. That would indicate an accelerated oxidation of the sulfide (S^{-2})

[1]Researcher, Institute of Fundamental Technological Research, Polish Academy of Sciences, Pawinskiego 5b, 02-106 Warsaw, Poland. *Corresponding author,
E-mail: mdabrow@ippt.pan.pl
[2]Professor, Institute of Fundamental Technological Research, Polish Academy of Sciences, Pawinskiego 5b, 02-106 Warsaw, Poland.
[3]Researcher, Institute of Fundamental Technological Research, Polish Academy of Sciences, Pawinskiego 5b, 02-106 Warsaw, Poland.
[4]Head of Laboratory of Experimental Physics and Nuclear Safety of Reactor Facilities, The Joint Institute for Power and Nuclear Research - Sosny of the National Academy of Sciences of Belarus, Minsk 220109, Belarus.
[5]Researcher, The Joint Institute for Power and Nuclear Research - Sosny of the National Academy of Sciences of Belarus, Minsk 220109, Belarus.

Table 1 Physical properties of aggregates determined using standard test methods.

Property	Amphibolite	Magnetite	Baryte
Density, kg/m^3 (PN-EN 1097-6, 2013)	2900	4800	4200
Water absorption, % (PN-EN 1097-6, 2013)0	0.7	1.1	0.2
Thermal conductivity, W/m·K (Jaskulski *et al.* 2019)	3.2	4.7	2.5
Specific heat, J/kg·K (Jaskulski *et al.* 2019)	670-1260	~600#)	~450#)

#) no data available for rocks, data for minerals

Table 2 Concrete mix design, kg/m^3.

Concrete designation	Cement		Water	Sand	Crushed aggregate		
					Amphibolite	Magnetite	Baryte
				0-2 mm	2-8 mm		
A	CEM II/B-S 42.5N	520	260	615	929	-	-
M					-	1537	
B					-	-	1345

supplied by the slag, to form sulfates (SO_4^{-2}) and promote further formation of ettringite due to gamma exposure. Both Craeye *et al.* (2015) and Mobasher *et al.* (2015) confirmed formation of ettringite under gamma irradiation for a slag-rich blended cement mortar. Additionally, the strength of irradiated mortars with slag was not compromised with cracks and open voids formed as a result of radiolytic dehydration. Such changes were not observed in the plain cement mortar.

Preliminary tests on the use of gamma radiation during the setting and early hardening of cement mortar revealed a tendency to increase the early strength (Khmurovska *et al.* 2020). The results indicate a local densification of cement matrix, resulting in reduced capillary porosity (Burnham *et al.* 2016). Therefore, some gamma radiation-induced changes of paste-aggregate contact zone can be expected. However no comprehensive study on the early gamma irradiation was published.

The goal of the current investigation is to determine the effects of gamma irradiation on the mechanical properties and porosity of concrete at the early age. Experimental tests are performed on hardening concrete specimens containing heavyweight magnetite and baryte aggregate that were exposed to gamma irradiation during the initial 16 hours after casting. The irradiated modulus of elasticity and porosity of early age concrete is studied in respect to the observations of microstructural features.

2. Experimental

2.1 Materials and specimens irradiation/curing

Cement CEM II/B-S 42.5N (PN-EN 197-1 2012), with blast furnace slag, characterized by a normal rate of strength growth, was used. Natural quartz sand (density 2.65 kg/dm^3), crushed aggregates from three rocks differing in mechanical properties and density were used: amphibolite, magnetite and baryte (the rock density of 2.90 kg/dm^3, 4.80 kg/dm^3 and 4.20 kg/dm^3, respectively). The above rocks differ also in the specific heat and thermal conductivity (**Table 1**).

Concrete mix was designed with a large excess of cement paste 428 dm^3/m^3 (cement 520 kg/m^3 and water to cement ratio of 0.50), so as to obtain an increased workability for different aggregate consistency. These three types of crushed rock aggregates were consistently used for design and testing of radiation shielding concrete (Kubissa and Glinicki 2017). The volume proportion of 0-2 mm fraction and 2-8 mm fraction was determined as 42% and 58%, respectively, based on the standard limit curves for aggregate gradation. The mix design is given in **Table 2**.

Concrete mixtures were cast in cylindrical polypropylene molds with a diameter of Φ = 100 mm and h = 200 mm and compacted by external vibration. The molds filled with concrete mix were wrapped in an impermeable foil to protect from moisture exchange with the surroundings. One hour after mixing the molds filled with concrete were placed vertically close to the gamma radiation source for 16 hours, which cover the intensive part of chosen cement hydration. The gamma radiation source was ^{60}Co Irradiation Facility UGU-420 of the Joint Institute for Power and Nuclear Research - Sosny of the National Academy of Sciences of Belarus (**Fig. 1**). Specimens were placed next to a steel sheet separating the radioactive fuel rods.

The gamma dose was measured by four sensors placed at the circumference of each cylinder at every 90°. The sensors were placed on the specimens in molds wrapped in foil. After each hour of exposure, the cylinders with concrete were rotated by 90° around the symmetry axis to ensure a uniform dose of radiation throughout the specimen. During 16 h of irradiation the dose of gamma exposure recorded by the sensors was 56 ± 3 kGy (the average of 4 measurements). The effect of the polypropylene mold on the gamma radiation dose in concrete is negligible and is included in the measurement uncertainty. The air temperature and the relative humidity in the radiation chamber was 15 ± 3°C and RH = 40 ± 10%, without any possibility of more precise control.

Additional specimens were prepared at IPPT PAN laboratory one day before gamma radiation experiment, designated L and cured in a climatic chamber to mimic the conditions in the radiation chamber (the temperature of 15 ± 3°C and RH = 40 ± 10%). The specimens were used to determine the cylinder compressive strength (f_{cm}) and confirm mixing repeatability with the main gamma irradiation experiment.

After irradiation, the concrete specimens in the molds, insulated against moisture exchange with the environment, were transported to IPPT PAN laboratory in Warsaw. The thermal conditions during transport were recorded using iButton temperature sensors – the temperature was fairly constant in the range of 17-21°C. 48 hours after concrete mixing the molds were unwrapped

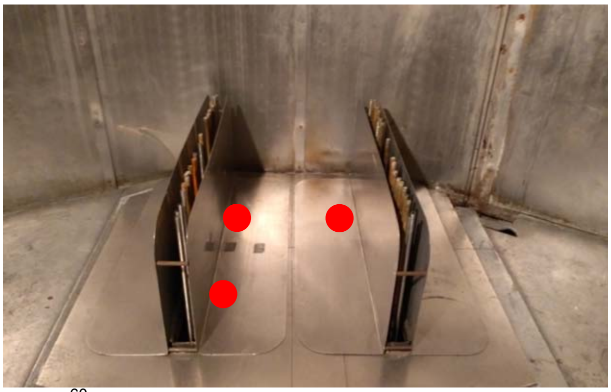

Fig. 1 ^{60}Co Irradiation chamber UGU-420 of the Joint Institute for Power and Nuclear Research – Sosny (red points – position of specimens).

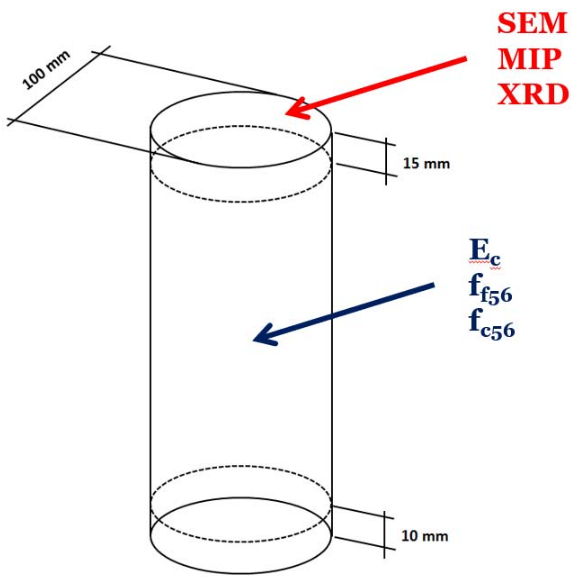

Fig. 2 Scheme of specimen sectioning for mechanical tests and microstructural characterization (f_{f56}, f_{c56} – flexural and compressive strength respectively, after 56 days of curing).

and the specimens were taken out. Next, the specimens were cut as shown in **Fig. 2** to obtain specimens for mechanical testing and microstructural evaluation.

2.2 Test methods

The determination of the secant modulus of elasticity (E_c) of concrete in compression was performed according to method A of PN-EN 12390-13 (2014), using Controls testing machine with the Automax Multitest console. Concrete cylindrical specimens Φ 100x171 mm were used after parallel grinding of base sides. To determine the lower stress level (σ_b = 0.1 f_{cm}) and the upper stress level ($\sigma_a = f_{cm}$ / 3), the column compressive strength (f_{cm}) was determined on specimens in climatic chamber to mimic the conditions in the radiation chamber. The tests were performed on specimens after 2, 3, 6, 9, 16, 23, 28, 35, 44 and 56 days of curing.

Three-point bending test was performed using LLOYD EZ 50 machine on prismatic concrete specimens 30x30x171 mm that were cut from the inner part of cylinder after testing the secant modulus of elasticity. For each concrete mix three specimens were tested at the loading rate of 50 N/s. Compressive strength test was performed using Controls machine at the rate of loading of 500 N/s on six specimens for each concrete mix. Additionally, the compressive strength (PN-EN 12390-3 2019) of three cubes 150 mm after 28 days of standard curing was measured.

Mercury intrusion porosity (MIP) measurements were carried out on mortar pieces separated from concrete cylinders. Specimens were dried at 50°C until a constant weight to avoid microcracks and then they were kept in sealed containers until the day of the test. The size of specimens for MIP analysis was linked to the size of measurement container of Quantachrome Poremaster 60 porosimeter. The porosimeter could detect the pores as small as 5 nm with the maximum pressure of 414 MPa. Measurements were performed on specimens after 7 days of drying.

The X-ray diffraction (XRD) method was used to analyze the mineral composition of the cement matrix separated from crushed part of concrete disc with some small grains of aggregate. A Bruker (Karlsruhe, Germany) D8 Discover diffractometer was used with a voltage ratio of 40 kV and 40 mA lamp current. A copper lamp was used as an X-ray source. The scan step size was 0.02°, collection time 1 s, and in the range 2Θ Cu Kα from 5 to 65°. All specimens were powdered after cutting from disk and sieved through a 0.045 mm sieve. Subsequently, the hydration arresting of cement was done by submerging in acetone for the next 48 h and drying for 7 days at 50°C before testing.

The microscopic examination was carried out on concrete specimens 25x15x10 mm cut from the cylinders. After drying in an oven at 50°C for 3 days, vacuum-impregnation with a low-viscosity epoxy, lapping and polishing, the specimens were coated with a thin layer of carbon. A JEOL JSM-6460 LV scanning electron

Table 3 Determination of the lower and upper stress level during the test of the secant modulus of elasticity.

Concrete designation	Curing time[days]	f_{cm} [MPa]			Average value [MPa]	Stand. dev [MPa]	σ_b [MPa]	σ_a [MPa]
		1	2	3				
A	2	15.2	14.5	14.9	14.9	0.3	2	4
	3	22.4	23.9	23.8	23.4	0.7	2	7
	6	34.9	32.1	33.5	33.5	1.1	3	10
	9	39.4	40.1	41.7	40.4	1.0	4	12
M	2	13.9	14.2	12.5	13.5	0.7	2	4
	3	19.6	20.3	21.2	20.4	0.7	2	6
	6	27.5	28.9	29.5	28.6	0.8	3	9
	9	35.8	36.1	33.4	35.1	1.2	4	11
B	2	14.5	14.9	12.5	14.0	1.0	2	4
	3	21.6	22.8	22.1	22.2	0.5	2	7
	6	30.1	31.9	29.1	30.4	1.2	3	9
	9	35.1	36.3	37.8	36.4	1.1	4	11

microscope (SEM) with an energy dispersive spectroscopy (EDS) was used in the backscatter mode using an acceleration voltage of 12 kV and a resolution of 3.0 nm. SEM observations were made using a magnification range of 30x to 1500x. The chemical composition was analysed using Genesis Spectrum 6.2 by EDAX Inc.

3. Test results and discussion

3.1 Mechanical properties

(1) Secant modulus of elasticity

To determine the lower and upper stress level needed to perform tests of elastic modulus, the compressive strength of concrete was measured after the intended curing period (**Table 3**). On this basis, the following stress ranges were assumed at the given age of concrete for all tested series:

At 2 days: $\sigma_b = 2$ MPa and $\sigma_a = 4$ MPa,
At 3 days: $\sigma_b = 2$ MPa and $\sigma_a = 6$ MPa,
At 6 days: $\sigma_b = 3$ MPa and $\sigma_a = 9$ MPa,
At 9 days and later: $\sigma_b = 4$ MPa and $\sigma_a = 11$ MPa.

The elastic modulus data are given in **Figs. 3-5**. The earliest measurements provided the most significant information about the influence of gamma radiation on the modulus of elasticity. The moisture condition of the specimens cured during the exposure to gamma radiation was the same for the examined aggregate variants. However, the measurement after 2 days and subsequent measurements were made at different moisture conditions of concrete specimens (the same for tested concrete series), which had a direct impact on the secant modulus of elasticity (E_c). After 2 days of curing at the reference laboratory conditions (L) the average secant modulus of elasticity was 20.6, 21.4 and 17.3 GPa for concrete with amphibolite, magnetite and baryte aggregate, respectively.

The exposure of specimens to gamma irradiation during the first 16 hours of 2 days curing resulted in an increase of E_c by 37%, 32% and 23% for concrete specimens with amphibolite, magnetite and baryte aggregates, respectively. The increased elastic modulus of gamma irradiated specimens was clearly observed during the first several days of concrete hardening. After 23 days of curing of magnetite concrete, the elastic modulus of early-irradiated specimens was equal to that of non-irradiated specimens. For two concrete series (A and B) the irradiation induced stiffening effect remained constant from the 6th day of curing to the end of the experiment. The E_c increase after early irradiation may be explained by a thermal effect of gamma radiation and subsequent increase in the degree of cement hydration (Mobasher *et al.* 2015). An increase of the compressive strength due to early gamma irradiation was reported in (Burnham *et al.* 2016). Other studies revealed a correlation with the modulus of elasticity of concrete (Huska *et al.* 2013; Alsalman *et al.* 2017). No systematic influence of the thermal properties of aggregates on E_c of early-irradiated concrete was observed.

(2) Flexural and compressive strength

The strength of concrete specimens after 56 days of curing is shown in **Fig. 6**. The flexural strength and compressive strength data show no significant effect of gamma irradiation of concrete specimens during early hardening stage. Strength tests were carried out on specimens cut from the inner part of irradiated cylinders, thus excluding external layer of concrete. Therefore, it actually means that no strengthening effect was found for the internal parts of concrete specimens exposed to early gamma irradiation.

Specimens of baryte concrete revealed smaller flexural and compressive strength than the strength of amphibolite or magnetite concrete by several to several dozen percent, respectively. Such an observation confirms the findings of other authors (Akkurt *et al.* 2005; Kilincarslan *et al.* 2006). It was due to small strength increase during the late hydration of slag cement in the presence of baryte aggregate (Ouda 2015), which was explained by the lower mechanical properties of baryte aggregate (Pomaro *et al.* 2019).

The compressive strength of magnetite concrete was about 60 MPa. Concretes with amphibolite and baryte were characterized by lower compressive strength by 9% and 33%, respectively. A similar relative strength difference was also observed in flexure strength measurements.

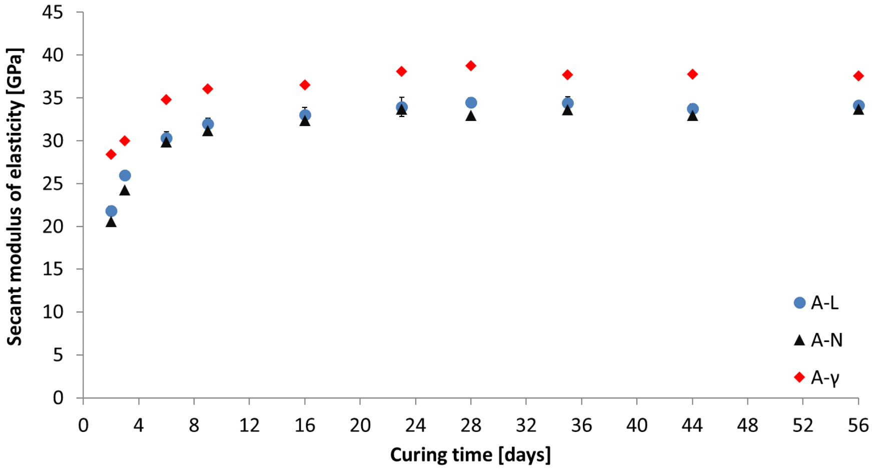

Fig. 3 The change of secant modulus of elasticity of concrete containing amphibolite aggregate with curing time at: laboratory simulated conditions at IPPT (A-L), laboratory conditions of UGU-420 without gamma exposure (A-N), the gamma irradiation chamber of UGU-420 (A-γ).

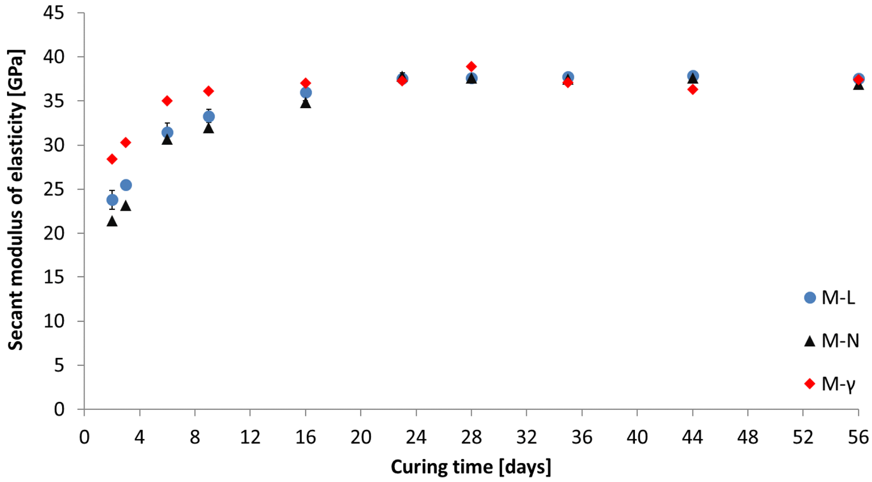

Fig. 4 The change of secant modulus of elasticity of concrete containing magnetite aggregate with curing time at: laboratory simulated conditions at IPPT (M-L), laboratory conditions of UGU-420 without gamma exposure (M-N), the gamma irradiation chamber of UGU-420 (M-γ).

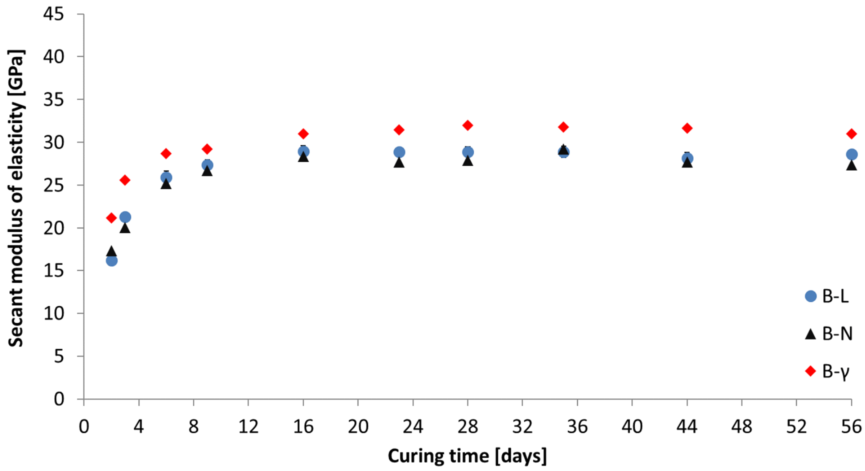

Fig. 5 The change of secant modulus of elasticity of concrete containing baryte aggregate with curing time at: laboratory simulated conditions at IPPT (B-L), laboratory conditions of UGU-420 without gamma exposure (B-N), the gamma irradiation chamber of UGU-420 (B-γ).

3.2 Pore size distribution

The MIP data obtained after 48 hours of curing of concrete with three types of aggregate are shown in **Figs. 7-9**. The reference specimens cured without gamma irradiation exhibited a capillary pore volume from 0.058 cm^3/g for baryte concrete to 0.079 and 0.083 cm^3/g for magnetite and amphibolite concrete, respectively. A reduced porosity of baryte concrete is due to the low hardness of baryte rock, that facilitates some crushing of aggregate grains into fines that fill the microvoids in a similar way as ground limestone (Wang *et al.* 2019). The distribution of capillary pore size in concrete cured for 48 hours shows a much larger share of pores in the range of 0.1-1 µm than in concrete cured 28 days. That is a confirmation of the increased early-age permeability of cement matrix (Zhang *et al.* 2018). The early exposure of specimens to gamma irradiation resulted in a reduction of the total capillary pore volume by 8%, 30% and 100% in the case of concrete with baryte, amphibolite and magnetite aggregate, respectively. A significant reduction of share of pores in the range of 0.1-1 µm was observed due to early irradiation. Also, it was found that the share of pores in the range of 0.01-0.1 µm increased due to early-irradiation and capillary pores with a diameter of about 0.1 µm became the most numerous pores.

3.3 Qualitative phase composition

The phase composition data obtain after 48 hours of curing are presented in **Figs. 10-12**. In the cement matrix separated from the concrete, peaks derived from aggregate minerals, i.n. quartz, amphibole, feldspar, plagioclase, magnetite and baryte were visible. The presence of typical crystalline hydration products was found, i.e., portlandite (d = 2.628, d = 4.902 Å), ettringite (d = 9.709 Å), monosulfate (d = 8.929 Å) and small amounts of clinker minerals, i.e. C_3S (d = 2.776 Å), C_2S (d = 2.744 Å), C_3A (d = 2.700 Å). Monosulfate was not

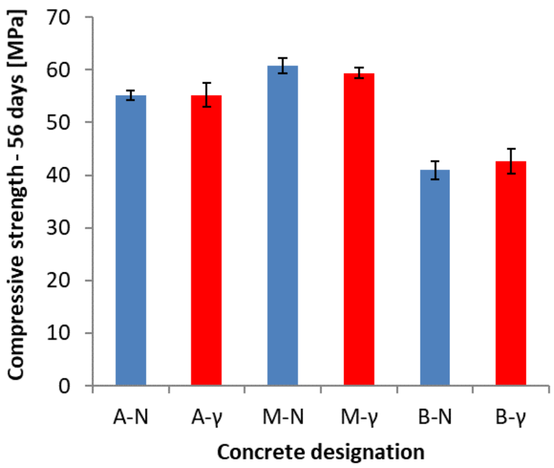

a)

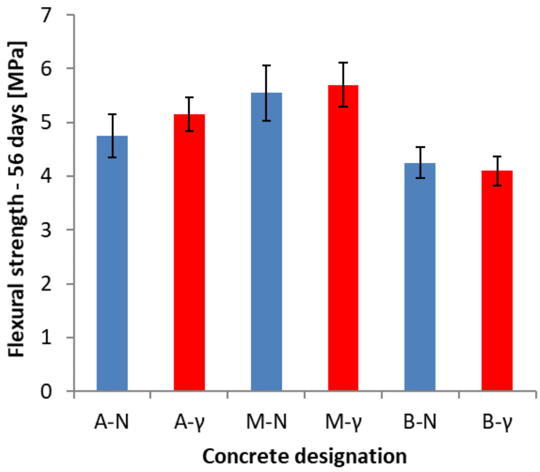

b)

Fig. 6 The influence of gamma irradiation on the strength of concrete with slag cement CEM II B-S after 56 days of curing: a) flexural strength, b) compressive strength.

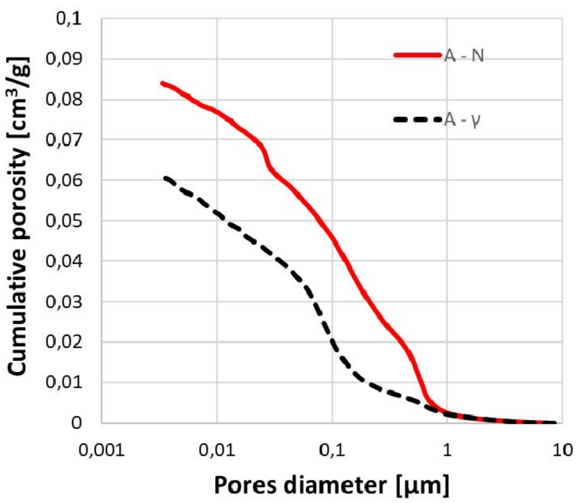

a)

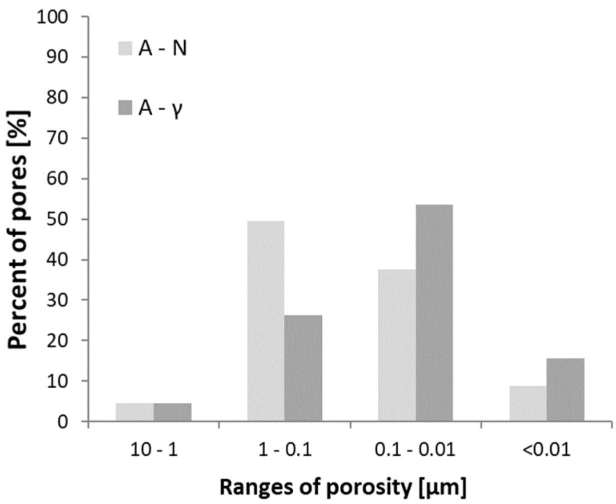

b)

Fig. 7 The influence of gamma irradiation on the pore size distribution in mortar fraction of concrete with amphibolite aggregate: a) total volume, b) percent of pores in selected ranges.

detected in the cement matrix taken from concrete with baryte aggregate. The hydration products that could appear in slag binders were not observed, i.e.: calcium peroxide octahydrate ($CaO_2 \cdot 8H_2O$), hydrotalcite ($Mg_6Al_2(CO_3)(OH)_{16} \cdot 4H_2O$) and calcite ($CaCO_3$) (Mobasher *et al.* 2015).

Figures 13 and **14** show a comparison of the characteristic portlandite peak (d = 2,628 Å and d = 4.902 Å) of all concrete mixes. The intensity of the portlandite peaks was small. There was no increase in the intensity of portlandite peaks in the cement matrix after the gamma-ray exposure and its decrease in the case of mixtures with amphibolite and magnetite was observed. In the case of the remaining crystalline products of hydration and non-hydrated clinker minerals in cement matrix, no differences between the irradiated and non-irradiated specimens were observed.

3.4 Microstructural features

The results of microscopic observations carried out on concrete specimens exposed to gamma irradiation and on reference specimens without irradiation are presented in **Figs. 15-18**. The major irradiation induced changes were visible in an external layer located about 1-2 mm from the edge of specimens subjected to irradiation, **Fig. 15**. The differences were detected in all specimens regardless of the coarse aggregate used, however, changes in the cement matrix related to irradiation reached the deepest in specimen with reference aggregate - magnetite and baryte, **Fig. 16**. Numerous unreacted cement grains and partly reacted cement and slag particles were found in reference specimens, **Fig. 15a**. Much less unreacted slag grains were found in irradiated concrete specimens, **Fig 15b**. The slag grains with a size < 20 µm were completely transformed into reaction products, while in larger grains the partially reacted zone was clearly visible.

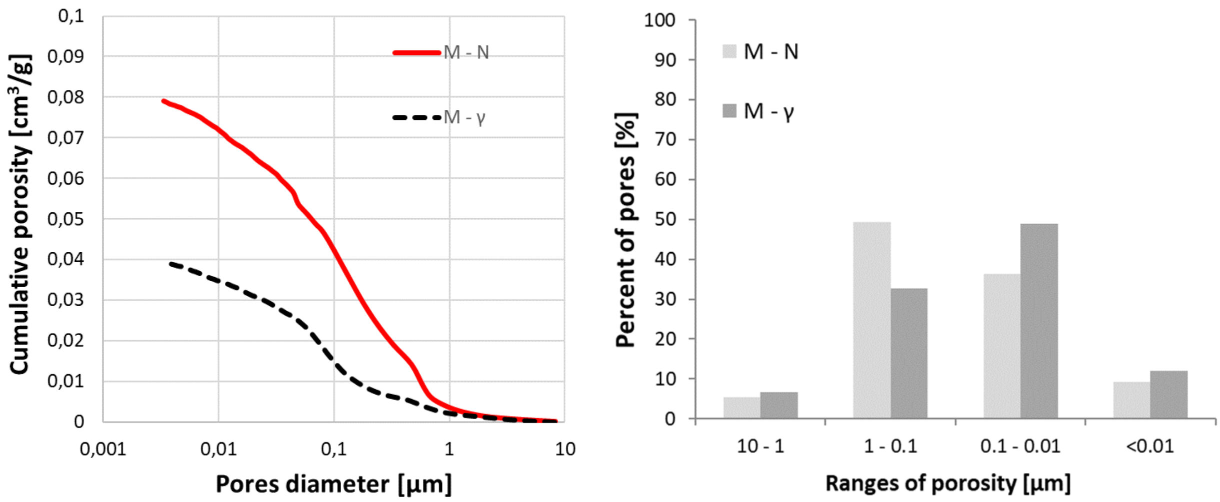

a) b)

Fig. 8 The influence of gamma irradiation on the pore size distribution in mortar fraction of concrete with magnetite aggregate: a) total volume, b) percent of pores in selected ranges.

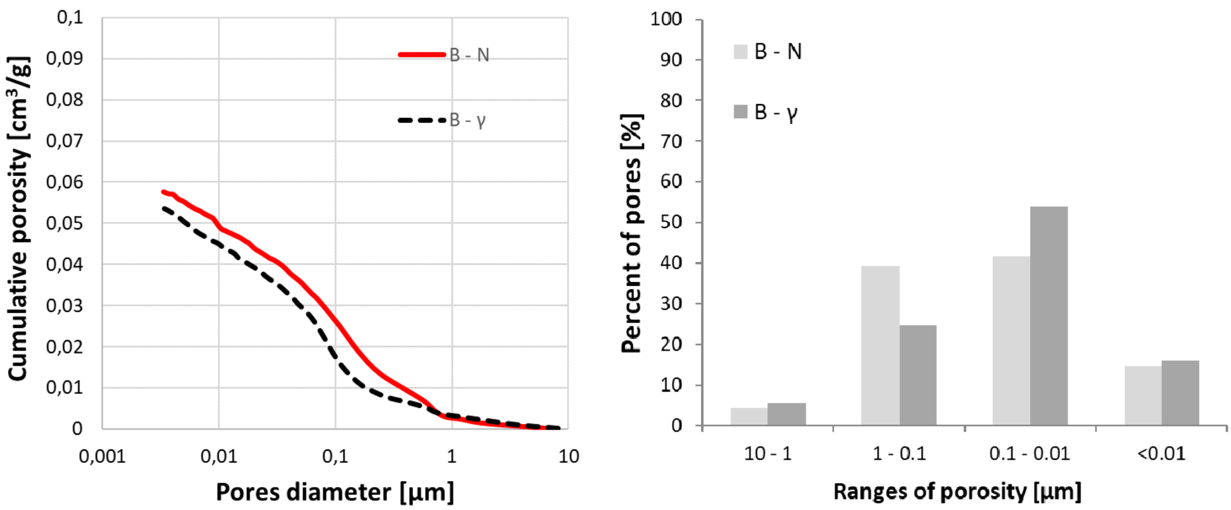

a) b)

Fig. 9 The influence of gamma irradiation on the pore size distribution in mortar fraction of concrete with baryte aggregate: a) total volume, b) percent of pores in selected ranges.

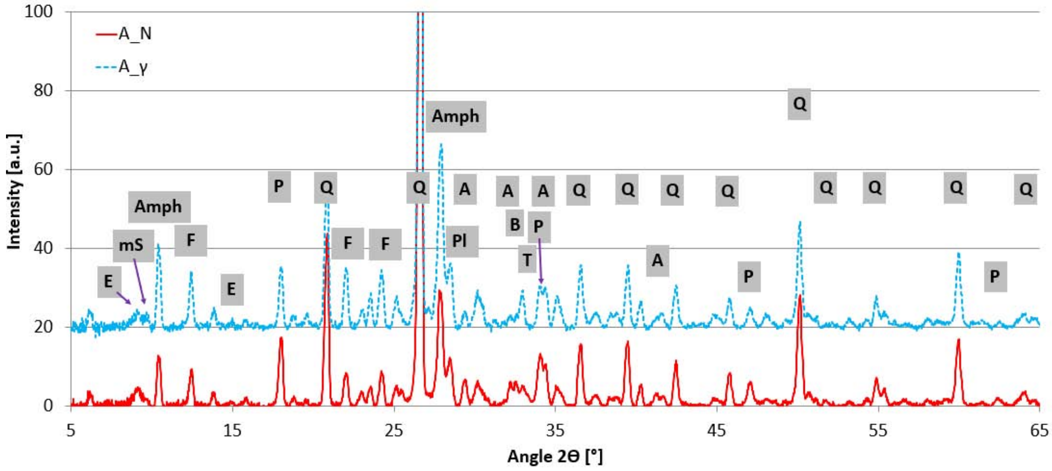

Fig. 10 The influence of early gamma irradiation on the phase composition cementitious matrix separated from concrete with amphibolite aggregate (Notation: A – C_3S , B – C_2S, T – C_3A, P – portlandite, E – ettringite, mS – monosulfate, Q – quartz, F – feldspar, Amph – amphibole, Pl – placioglase).

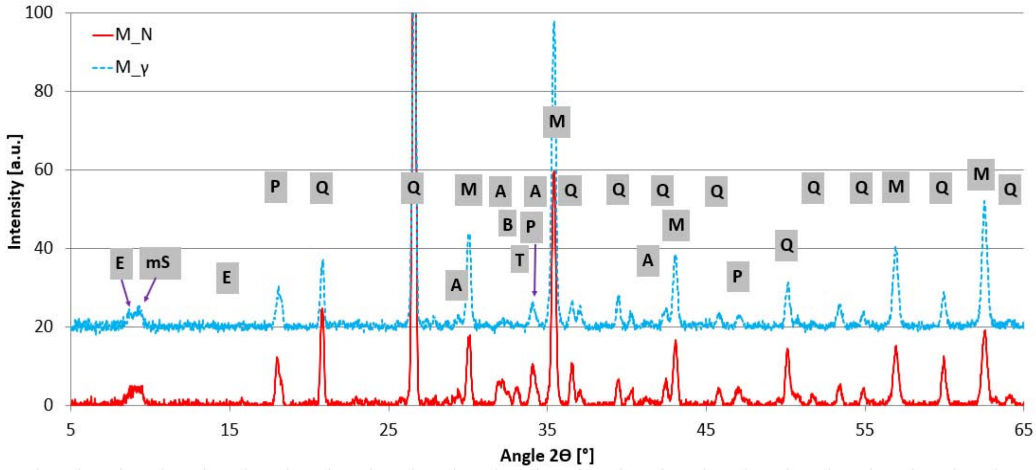

Fig. 11 The influence of early gamma irradiation on the phase composition cementitious matrix separated from concrete with magnetite aggregate (Notation: A – C_3S , B – C_2S, T – C_3A, P – portlandite, E – ettringite, mS – monosulfate, Q – quartz, M – magnetite).

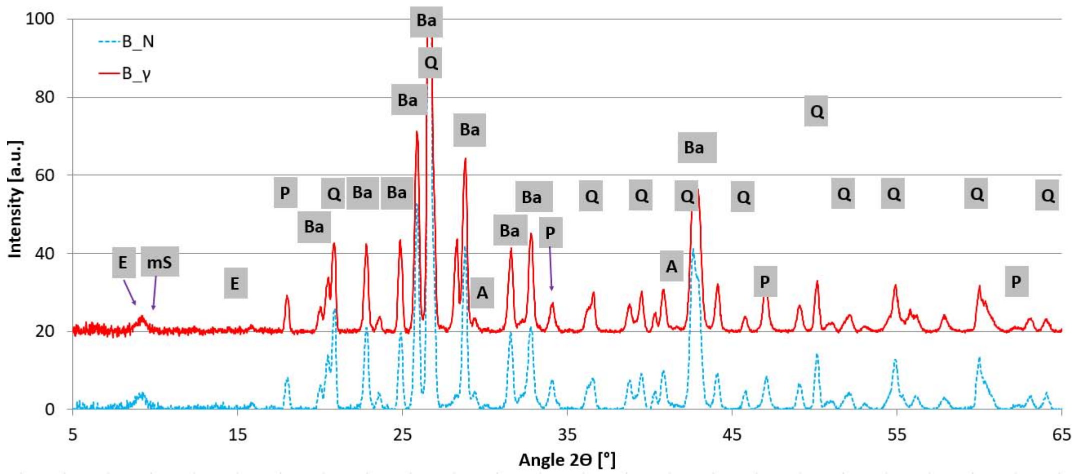

Fig. 12 The influence of early gamma irradiation on the phase composition cementitious matrix separated from concrete with baryte aggregate (Notation: A – C_3S , B – C_2S, T – C_3A, P – portlandite, E – ettringite, mS – monosulfate, Q – quartz, Ba – baryte).

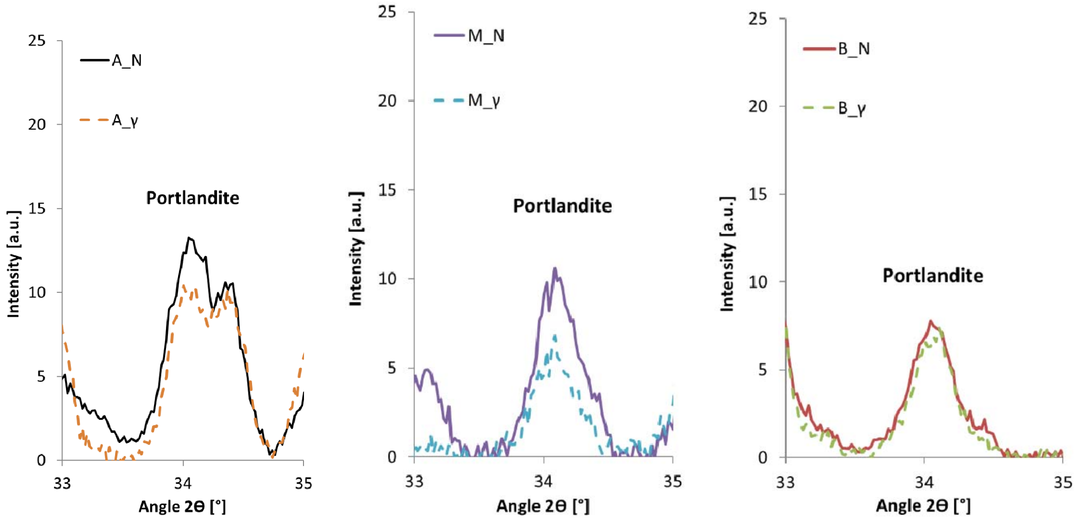

(a) (b) (c)

Fig. 13 The influence of early gamma irradiation on portlandite intensity (d = 2.628 Å) in the matrix separated from concrete with amphibolite (a) magnetite (b) and baryte (c) aggregate.

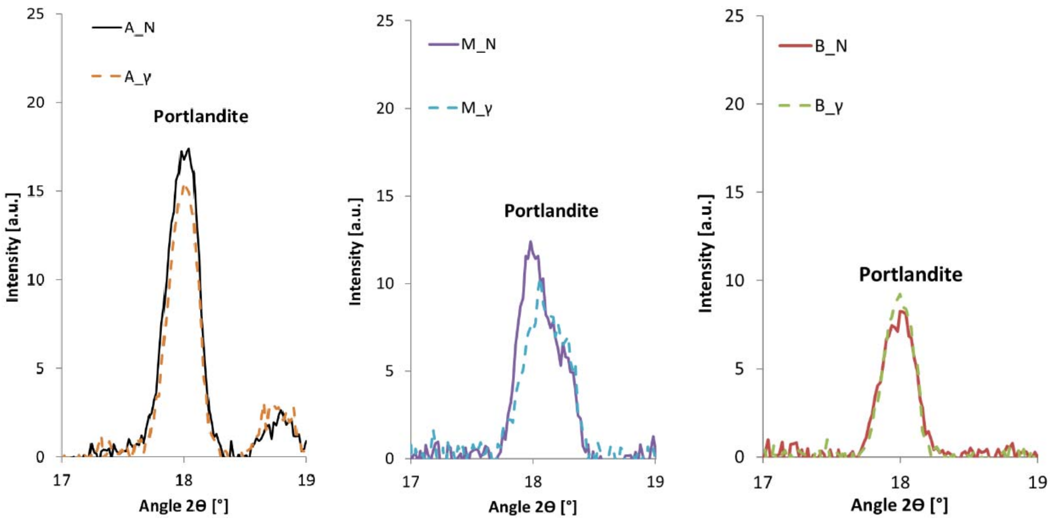

(a) (b) (c)

Fig. 14 The influence of early gamma irradiation on portlandite intensity (d = 4,902 Å) in the matrix separated from concrete with amphibolite (a) magnetite (b) and baryte (c) aggregate.

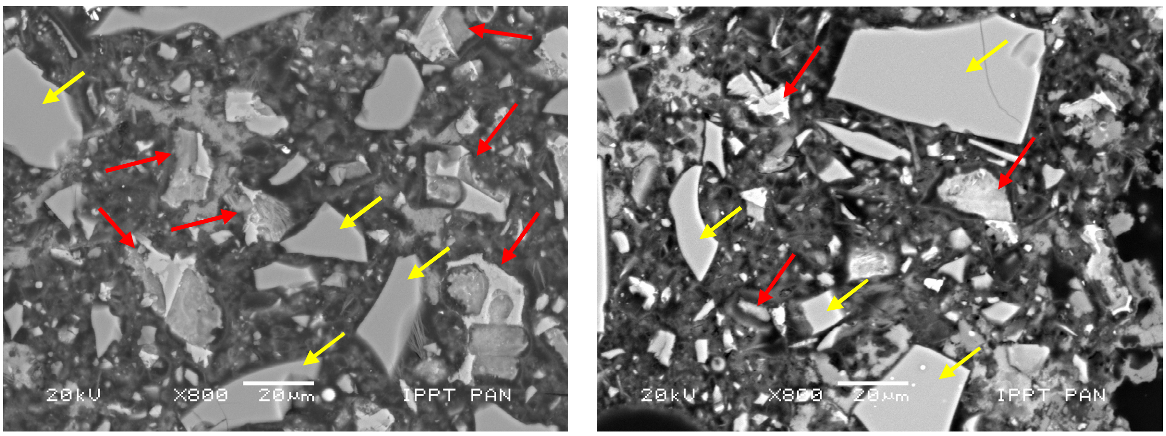

(a) (b)

Fig. 15 SEM images of magnetite concrete at the external layer of specimen: a) not irradiated, b) irradiated (the scale bar 20 μm; the red arrows mark partially reacted cement grains; yellow arrows – slag particles).

In reference concrete specimens unreacted slag grains, regardless of their size, were visible, as well as non-hydrated cement grains with visible alite, belite and ferrite phases, **Fig. 16**. The irradiated specimens were characterized by a well visible presence of portlandite in cement matrix, more abundant in comparison to non-irradiated specimens. At the same time, in the specimens exposed to gamma irradiation, the presence of portlandite in the matrix decreased with increasing distance from the edge of the specimen to its center, **Fig. 17**. SEM-EDS analysis in micro-areas did not reveal any differences in chemical composition of portlandite. In irradiated specimens the abundant presence of monosulfate was found at the external edges of specimens, while in

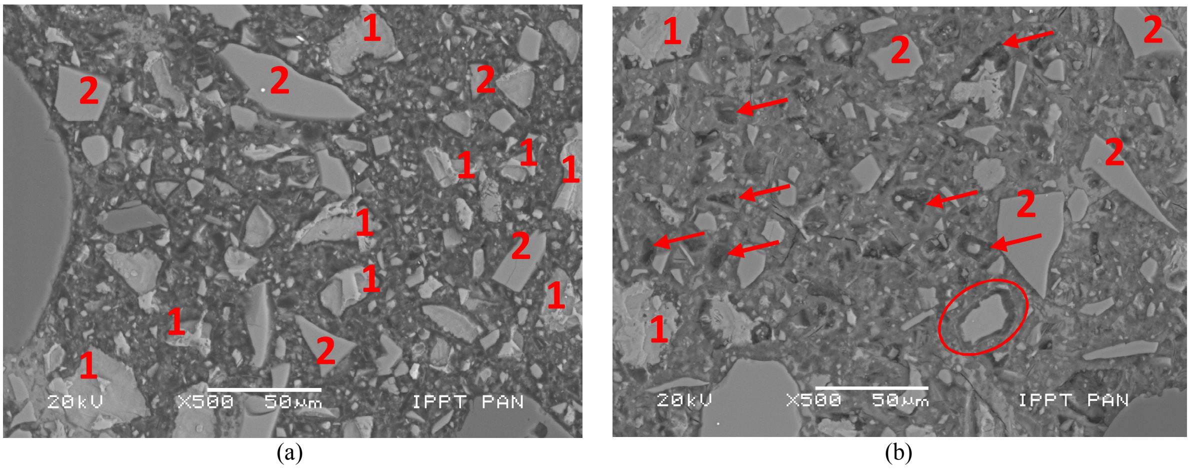

Fig. 16 SEM images of amphibolite concrete in the middle of the specimen: (a) not irradiated, (b) irradiated (the scale bar = 50 µm, the arrows indicate the partly reacted slag grains, 1-cement, 2-slag).

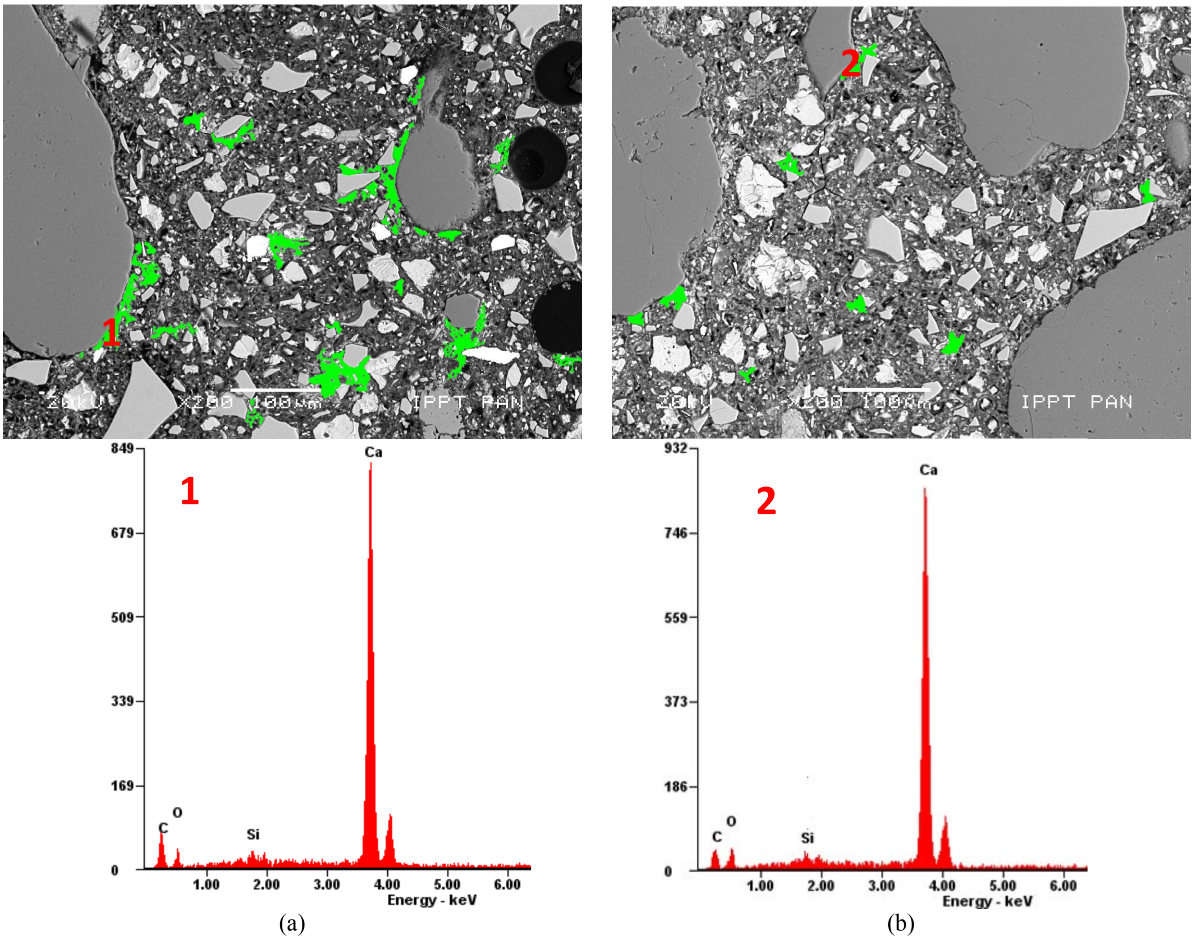

Fig. 17 SEM-EDS images of irradiated concrete with magnetite aggregate: (a) the layer up to 2 mm from the edge of the specimen, (b) 25 mm from the edge of the specimen (the scale bar 100 µm; the green area corresponds to portlandite.)

reference specimens, the presence of monosulfate in the cement matrix was insignificant.

Microscopic observations of the aggregate-cement paste contact zone revealed also the visible effects of gamma irradiation during early hardening of concrete. As illustrated in **Fig.18**, in the area near to the edge of irradiated specimens, this zone was very compact, while in deeper regions (over 20 mm), zones of discontinuity between the aggregate and the cement matrix were observed. In the aggregate-paste contact zone the presence of portlandite was evident in all types of specimens.

4. Discussion

The obtained the secant modulus of elasticity values are comparable with the results of Shariq *et al.* (2013), where for normal weight concrete with w/c = 0.50 and the addition of the corresponding amount of blast furnace slag, E_c was about 15-18 GPa after 3 days of curing for samples in the surface dry condition. After 28 days of curing, depending on the aggregate type, the elastic modulus of Portland cement concrete ranges from 30 to 40 GPa (Hussain *et al.* 2018; Gonzalez-Ortega *et al.* 2014). An addition of up to 40% of slag may decrease E_c even by over 20% (Siddique and Kaur 2012). However, a long term curing of concrete with slag ensures E_c at the same level as concrete without such additive (Megat Johari *et al.* 2011). The moderate growth rate of E_c with time of curing was characteristic for concrete with the addition of granulated blast furnace slag (Shariq *et al.* 2013; Nassif *et al.* 2005).

The elastic modulus of concrete with iron-bearing aggregates, such as hematite and magnetite, is within the range of 27-60 GPa (Hussain *et al.* 2018; Lotfi-Omran *et al.* 2019), and with baryte aggregate 25-40 GPa (Hussain *et al.* 2018; Özbay *et al*. 2016; Gökçe *et al*. 2018). A wide range of E_c results from variability of rock properties and aggregate contents in concrete (Gökçe *et al.* 2018; Saidani *et al*. 2015). The current data range from 27 to 37 GPa correspond well with the literature data. The obtained strength data also confirm the known relationship between the secant modulus of elasticity and the compressive strength (Huska *et al.* 2013; Alsalman *et al.* 2017). Such a linear relationship E_c-f_{cm} is also found for irradiated concrete specimens with the same directional coefficient and a 4.5 GPa constant shift due to irradiation.

The development of the elastic modulus of concrete in time at prescribed curing conditions is described by numerous phenomenological models (Ausweger *et al.*

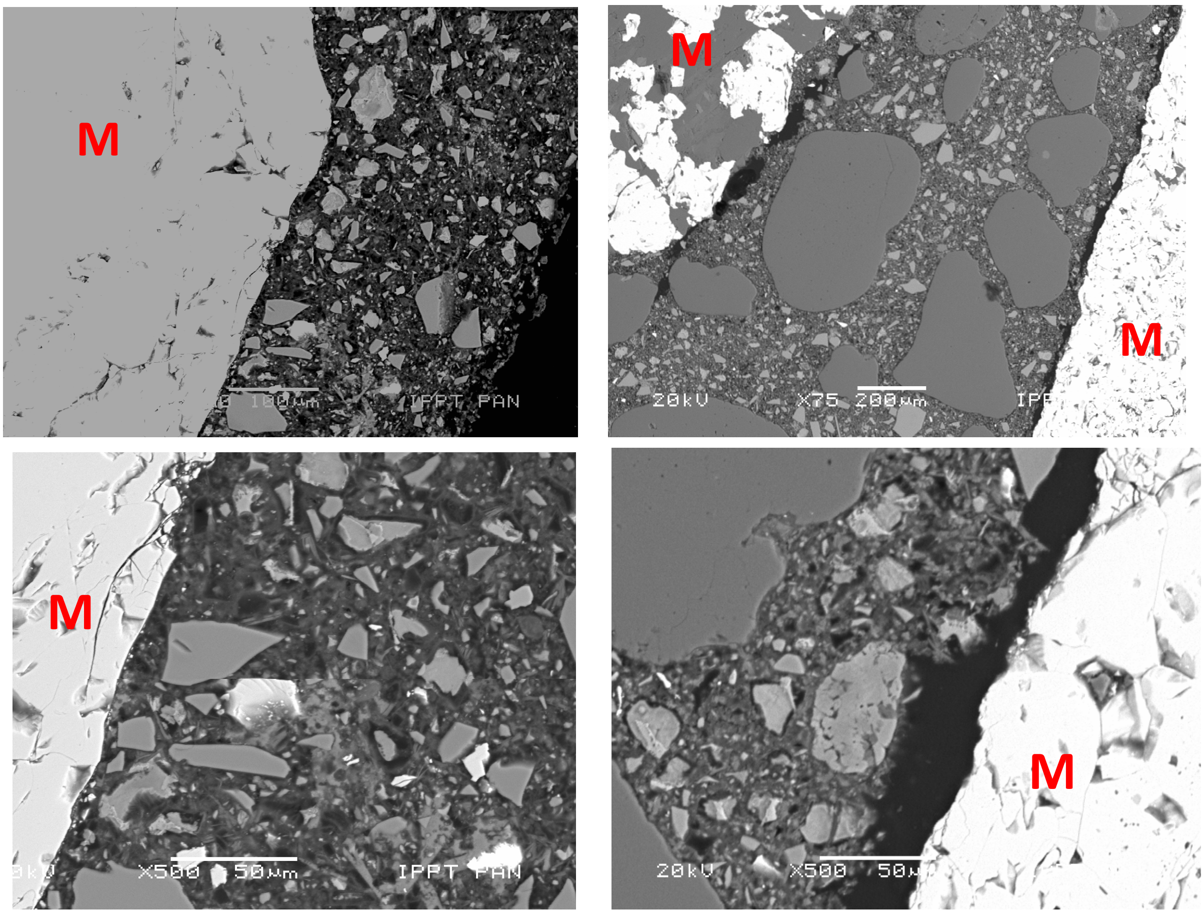

(a) (b)

Fig. 18 SEM images of aggregate-paste contact zone in irradiated concrete with magnetite aggregate: (a) up to 2 mm from the edge of the specimen, (b) 20 mm from the edge of the specimen (M-magnetite).

Table 4 Coefficients for elastic modulus prediction for concrete containing amphibolite, magnetite and baryte aggregates in laboratory curing conditions after 28 days of curing and for prediction of early gamma-irradiation effects.

Concrete designation, aggregate	Specific density [kg/dm^3]	Experimental data (average)		α_E	$k_{\gamma 1}$	$k_{\gamma 2}$
		E_{ci} [GPa]	$f_{cm,\ cube}$ [MPa]			
A-L amphibolite	2.9	34.5	66.3	0.92	1.125	1.319
B-L baryte	4.2	28.9	51.1	0.84	1.107	1.289
M-L magnetite	4.8	37.6	73.7	0.97	1.035	1.224

2019; Noguchi *et al.* 2009; *fib* 2010; ACI-318-08 2008), however no formulas include the relevant effects of gamma irradiation. While the elastic properties at fully hardened state are heavily dependent on the elastic properties of aggregate, at early ages such properties are mostly dependent on the rate of cement hydration and the early age elastic modulus of cementitious matrix. Such a distinction of kinetics of concrete stiffening is a basis for *fib* Model Code (2010) formulas. The elastic modulus of normal weight concrete at the age of 28 days (E_{ci}) [MPa] is given:

$$E_{ci} = 21500 \cdot \alpha_E \cdot \left(\frac{f_{cm}}{10}\right)^{\frac{1}{3}} \tag{1}$$

where, f_{cm} - the mean value of cylinder compressive strength in [MPa] of concrete age of 28 days, α_E – a dimensionless coefficient that accounts for the stiffness of aggregates (from 0.7 for sandstone to 1.2 for basalt).

An early age evolution of the elastic modulus in time ($E_c(t)$) is described by formula (2) during the first 28 days of curing at 20°C in high humidity conditions:

$$E_c(t) = E_{ci} \cdot \sqrt{\exp\left[s \cdot \left(1 - \sqrt{\frac{28}{t}}\right)\right]} \tag{2}$$

where, s – the coefficient which depends on the strength class of cement and the rate of its development (from 0.2 to 0.38 for high and low strength class respectively), t - the concrete age in days.

The curing conditions differences during early hardening of concrete are taken into consideration by adjusting the concrete age (t_T) according to equation (3) (*fib* 2010):

$$t_T = \sum_{i=1}^{n} \Delta t_i \cdot \exp\left[13.65 - \frac{4000}{273 + T(\Delta t_i)}\right] \tag{3}$$

where, Δt_i - is the number of days where a temperature T prevails, and $T(\Delta t_i)$ - is the temperature in [°C] during the time period Δt_i.

The experimental data presented in section 3.1 were used to calculate the coefficient α_E for three types of aggregate (**Table 4**) according to (1). Assuming the coefficient $s = 0.25$ for the cement strength class 42.5N (PN-EN 197-1) and taking into consideration the curing temperature, the elastic modulus was calculated using (2) and (3) (**Fig. 19**). In comparison to experimental data the predicted E_c grows faster during the first three days of curing. It confirms the prediction of elastic modulus by Shariq *et al.* (2013), showing a decrease of early concrete stiffening caused by a slag addition to concrete. The fit up to 28 days of curing is very good.

On the basis of experimental observations, to account for early age gamma irradiation of concrete, the formulas (1) and (2) are modified by new coefficients $k_{\gamma 1}$ and $k_{\gamma 2}$, respectively. The first one is assumed to account for the stiffness of the aggregate-paste contact zone. The second one is considered as an acceleration coefficient for early cement hydration. Therefore, the modified formulas are given as:

$$E'_{ci} = 21500 \cdot \alpha_E \cdot k_{\gamma 1} \cdot \left(\frac{f_{cm}}{10}\right)^{\frac{1}{3}} \tag{4}$$

$$E'_c(t) = E'_{ci} \cdot \sqrt{\exp\left[(k_{\gamma 2})^{-1} \cdot s \cdot \left(1 - \sqrt{\frac{28}{t}}\right)\right]} \tag{5}$$

The irradiation-induced stiffening coefficient $k_{\gamma 1}$ can be calculated as a ratio of elastic modulus of concrete exposed to irradiation ($E_{c28\gamma}$) and cured in laboratory conditions (E_{c28L}) after 28 days of curing:

$$k_{\gamma 1} = \frac{E_{c28\gamma}}{E_{c28L}} \tag{6}$$

Calculation of the irradiation-induced acceleration coefficient $k_{\gamma 2}$ is possible as a ratio of early elastic modulus of concrete exposed to irradiation ($E_{c2\gamma}$) and cured in laboratory conditions (E_{c2L}), i.e., after 2 days (at the time of the first possible measurements):

$$k_{\gamma 2} = \frac{E_{c2\gamma}}{E_{c2L}} \tag{7}$$

The coefficients $k_{\gamma 1}$ and $k_{\gamma 2}$ calculated for different types of aggregate in concrete are given in **Table 4**. Using these coefficients, a more accurate prediction of the development of elastic modulus of concrete exposed to early-age irradiation is obtained (**Fig. 20**). Both $k_{\gamma 1}$ and $k_{\gamma 2}$ coefficients are seen to decrease slightly with increasing density of aggregate. This comes as no surprise because of known gamma-attenuation efficiency related to the content of heavy elements in shielding material reflected by the half layer value.

For small gamma doses the crystalline structure of aggregate minerals is not expected to change significantly (Ichikawa and Koizumi 2002) and thermal effects from ionizing dispersion by elements with a large atomic mass can also be observed (Rosseel *et al.* 2016). The use of aggregate with an increased content of high-density elements in concrete increases the attenuation of gamma radiation (Kurtis *et al.* 2017; Le Pape *et al.* 2016). That explains the microstructure changes induced by irradiation (a more abundant presence of portlandite and completely reacted small slag grains) were observed at a greater depth for normal weight concrete. For heavyweight aggregate concrete, the irradiation affected zone was thinner. In consequence the stiffening effect represented by early E_c increase (2 days) was the highest in amphibolite concrete, even though the irradiation affected zone of only 1-2 mm was detected.

The reduction of capillary porosity as a result of early gamma irradiation was found in more distant areas from the external perimeter of specimens. It can be explained (Reches 2019b) as an effect of the locally increased temperature, leading to a greater degree of cement hydration in the inner part of the specimen.

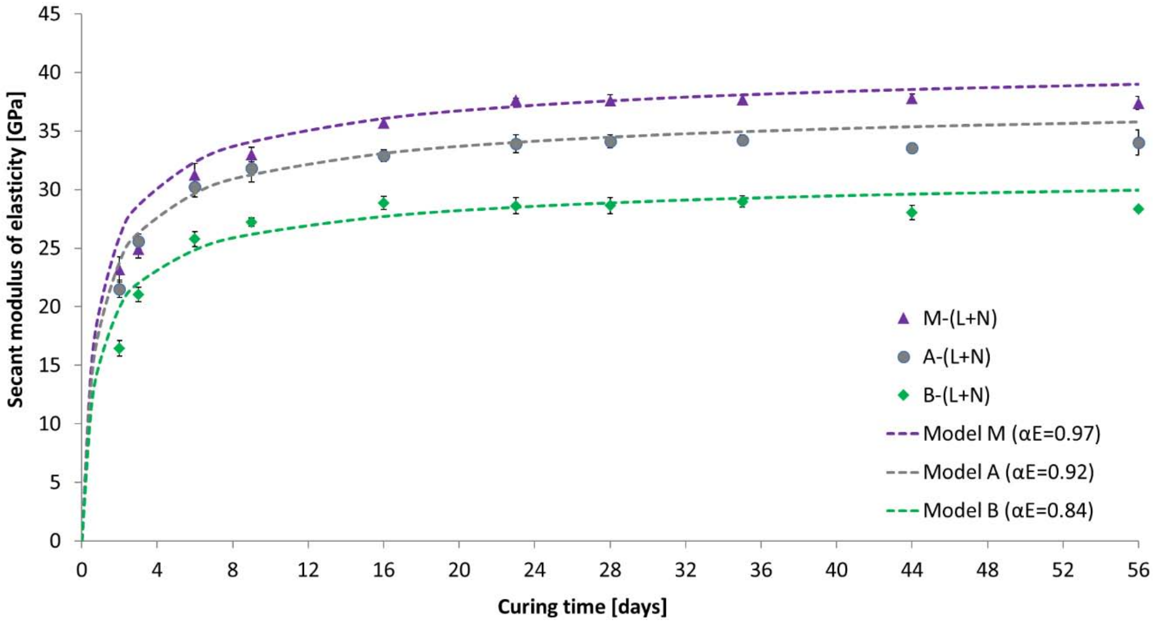

Fig. 19 The development of elastic modulus of nonirradiated concrete with amphibolite, magnetite and baryte aggregate with the curing time – experimental data and prediction.

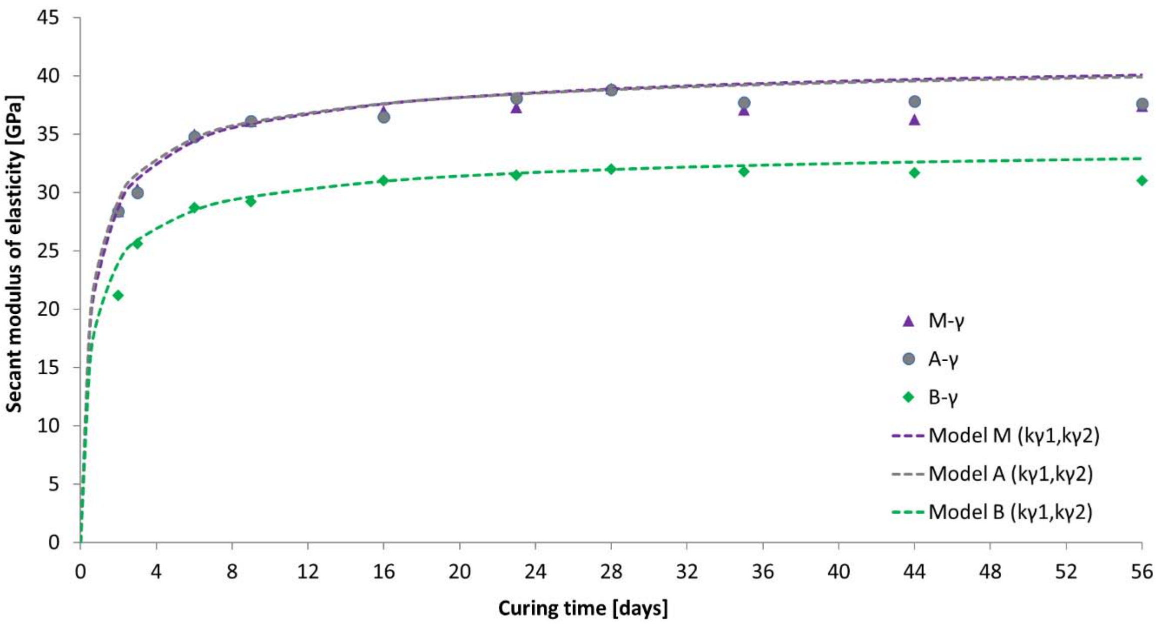

Fig. 20 The development of elastic modulus of early-irradiated concrete with amphibolite, magnetite and baryte aggregate with the curing time – experimental data and prediction according to (4) and (5) formulas.

Reported effects of gamma irradiation of early hardening concrete are beneficial for the development of mechanical properties at early ages. That was in contrast to reported negative effects of gamma irradiation like the formation of cracks, an increase in the volume of capillary pores and a decrease in strength, principally caused by gamma-induced drying of cementitious matrix. The significance of moisture conditions is confirmed once again.

5. Conclusions

The following conclusions can be drawn on the basis of the performed experimental investigation:

1) The exposure of early hardening concrete with amphibolite, magnetite and baryte aggregates to gamma irradiation up to 56 kGy resulted in an increase of the static modulus of elasticity at 48 hours by 37%, 32% and 23% respectively.
2) After 56 days of curing the modulus of elasticity of early-irradiated concrete with amphibolite and baryte aggregate was increased by 12% and 13%, respectively, while for magnetite concrete, the stiffening effect disappeared after 23 days of curing.
3) Early-age exposure to gamma irradiation had no significant influence on the flexural strength and compressive strength of concrete cut from interior part of cylinders after 56 days of curing under laboratory conditions, irrespective of aggregate type.
4) The relationship between the compressive strength and the secant modulus of elasticity of early-irradiated concrete is characterized by a shift of 4.5 GPa towards higher the modulus of elasticity without changing the directional factor.
5) Gamma early-irradiation reduced the capillary pore content by 8%, 30% and 100% for concrete containing baryte, amphibolite and magnetite aggregate, respectively. The irradiation enhanced the presence of a dominant group of capillary pores within the range from 0.05 to 0.2 μm.
6) Qualitative effects of gamma early-irradiation were detected in cement matrix in the surface layer up to the depth of 2 mm in concrete containing heavy aggregate. These were demonstrated by a visible higher degree of cement reaction with no unhydrated cement grains, a complete reaction of slag particles smaller than 20 μm, as well as more abundant portlandite crystals and the appearance of significant amounts of calcium monosulfate hydrate crystals.
7) The deeper penetration of gamma rays in cement matrix was found in concrete containing amphibolite aggregate in comparison to heavyweight concrete. This was especially evident in relation to the hydration of slag particles.
8) The cement matrix-aggregate contact zone in the early-irradiated concrete with magnetite aggregate showed the greatest difference between the surface zone, which was compact and without cracks, and the interior of the specimen with an increased number of voids and the discontinuity zone between grains and cement matrix.

Acknowledgements
The financial support by Polish National Centre for Research and Development (Project V4-Korea/2/2018) is gratefully acknowledged.

References

ACI, (2008). "*Building code requirements for structural concrete*, (ACI-318-08)." Farmington Hills, MI: American Concrete Institute.

Akkurt, I., Basyigit C., Kilincarslan, S. and Mavi, B., (2005). "The shielding of γ-rays by concretes produced with baryte." *Progress in Nuclear Energy*, 46(l), 1-11.

Alsalman, A., Dang, C. N., Prinz, G. S. and Hale, W. M., (2017). "Evaluation of modulus of elasticity of ultra-high performance concrete." *Construction and Building Materials*, 153, 918-928.

Ausweger, M., Binder, E., Lahayne, O., Reihsner, R., Maier, G., Peyerl, M. and Pichler, B., (2019). "Early-age evolution of strength, stiffness, and non-aging creep of concretes: experimental characterization and correlation analysis." *Materials*, 12, 207.

Bouniol, P. and Aspart, A., (1998). "Disappearance of oxygen in concrete under irradiation: the role of peroxides in radiolysis." *Cem. Concr. Res.*, 28(11), 1669-1681.

Burnham, S., Huang, L. and Jevremovic, T., (2016). "Examining the effect of gamma radiation exposure in early stage of concrete curing on its strength and long-term durability." In: *Proc. 24th International Conference on Nuclear Engineering*, edited by American Society of Mechanical Engineers, V005T15A068-V005T15A068.

Craeye, B., De Schutter, G., Van Humbeeck, H. and Van Cotthem, A., (2009). "Early age behaviour of concrete supercontainers for radioactive waste disposal." *Nuclear Engineering and Design*, 239, 23-35.

Craeye, B., De Schutter, G., Vuye, C. and Gerardy, I., (2015). "Cement-waste interactions: hardening self-compacting mortar exposed to gamma radiation." *Prog. Nucl. Energy*, 83, 212-219.

Gökçe, H. S., Yalçınkaya, Ç. and Tuyan, M., (2018). "Optimization of reactive powder concrete by means of baryte aggregate for both neutrons and gamma rays." *Construction and Building Materials*, 189, 470-477.

González-Ortega, M. A., Segura, I., Cavalaro, S. H. P., Toralles-Carbonari, B., Aguado, A. and Andrello A. C., (2014). "Radiological protection and mechanical properties of concretes with EAF steel slags." *Construction and Building Materials*, 51, 432-438.

Huska, P., Kolisko, J., Vokac, M. and Rehacek, S., (2013). "Test and technological influences on modulus of elasticity of concrete – recapitulation."

Procedia Engineering, 65, 266-272.

Hussain, R. R., Shuraim, A. B., Aslam, F., Alhozaimy, A. M. A., and Al-Humaiqani, M. M., (2018). "Coupled effect of coarse aggregate and micro-silica on the relation between strength and elasticity of high performance concrete." *Construction and Building Materials*, 175, 321-332.

Ichikawa, T. and Koizumi, H., (2002). "Possibility of radiation-induced degradation of concrete by alkali-silica reaction of aggregates." *Journal of Nuclear Science and Technology*, 39(8), 880-884.

fib, (2010). "*fib model code for concrete structures*." Berlin, Germany: Fédération Internationale du Béton.

Jaskulski, R., Glinicki, M. A., Kubissa, W. and Dąbrowski, M., (2019). "Application of a non-stationary method in determination of the thermal properties of radiation shielding concrete with heavy and hydrous aggregate." *International Journal of Heat and Mass Transfer*, 130, 882-892.

Khmurovska, Y., Štemberk, P., Sikorin, S.,Němeček, J., Jóźwiak-Niedźwiedzka, D., Doleželová, M., Kaladkevich, Y., Pavalanski, E., Fatseyeu, V., (2020). "Effects of gamma ray irradiation on hardened cement mortar." *International Journal of Concrete Structures and Materials*, 15(1).

Kilincarslan, S., Akkurt, I. and Basyigit, C., (2006). "The effect of baryte rate on some physical and mechanical properties of concrete." *Materials Science and Engineering: A*, 424, 83-86.

Kubissa, W. and Glinicki, M. A., (2017). "Influence of internal relative humidity and mix design of radiation shielding concrete on air permeability index." *Construction and Building Materials*, 147, 352-361.

Kurtis, K., Xi, Y., Glinicki, M. A., Provis, J., Giannini, E. and Fu, T., (2017). "Can we design concrete to survive nuclear environments?" *Concrete International*, 39(11), 29-35.

Le Pape, Y., Giorla, A. and Sanahuja, J., (2016). "Combined effects of temperature and irradiation on concrete damage." *Journal of Advanced Concrete Technology*, 14(3), 70-86.

Lotfi-Omran, O., Sadrmomtazi, A. and Nikbin, I. M., (2019). "A comprehensive study on the effect of water to cement ratio on the mechanical and radiation shielding properties of heavyweight concrete." *Construction and Building Materials*, 229, 116905.

Maruyama, I., Haba, K., Sato, O., Ishikawa, S., Kontani, O. and Takizawa, M., (2016). "A numerical model for concrete strength change under neutron and gamma-ray irradiation." *Journal of Advanced Concrete Technology*, 14(4), 144-162.

Maruyama, I., Ishikawa, S., Yasukouchi, J., Sawada, S., Kurihara, R., Takizawa, M. and Kontani, O., (2018). "Impact of gamma ray irradiation on hardened white Portland cement pastes exposed to atmosphere." *Cem. Concr. Res.*, 108, 59-71.

Megat Johari, M. A., Brooks, J. J., Kabir, S. and Rivard P., (2011). "Influence of supplementary cementitious materials on engineering properties of high strength concrete." *Constr. Build. Mater.*, 25, 2639-2648.

Mobasher, N., Bernal, S. A., Kinoshita, H., Sharrad, C. A. and Provis, J. L., (2015). "Gamma irradiation resistance of an early age slag-blended cement matrix for nuclear waste encapsulation." *J. Mater. Res.*, 30(9), 1563-1571.

Mobasher, N., Bernal, S. A., Kinoshita, H. and Provis, J. L., (2017). "Gamma irradiation resistance of early age $Ba(OH)_2$-Na_2SO_4-slag cementitious grouts." *Journal of Nuclear Materials*, 482, 266-277.

Noguchi, T., Tomosawa, F., Nemati, K. M., Chiaia, B. M. and Fantilli, A. P., (2009). "A practical equation for elastic modulus of concrete." *ACI Structural Journal*, 106, 690-696.

Nassif, H. H., Najm, H. and Suksawang, N., (2005). "Effect of pozzolanic materials and curing methods on the elastic modulus of HPC." *Cem. Concr. Compos.*, 27, 661-670.

Ouda, A. S., (2015) "Development of high-performance heavy density concrete using different aggregates for gamma-ray shielding." *Progress in Nuclear Energy*, 79, 48-55.

Özbay, E., Erdemir, M. and Durmus, H. I., (2016). "Utilization and efficiency of ground granulated blast furnace slag on concrete properties - A review." *Construction and Building Materials*, 105, 423-434.

PN-EN 1097-6, (2013). "*Tests for mechanical and physical properties of aggregates. Determination of particle density and water absorption*." Warszawa: The Polish Committee for Standardization (Polski Komitet Normalizacyjny – PKN).

PN-EN 12390-3, (2019). "*Testing hardened concrete. Compressive strength of test specimens*." Warszawa: The Polish Committee for Standardization (Polski Komitet Normalizacyjny – PKN).

PN-EN 12390-13, (2014). "*Testing hardened concrete - Part 13: Determination of secant modulus of elasticity in compression*." Warszawa: The Polish Committee for Standardization (Polski Komitet Normalizacyjny – PKN).

PN-EN 197-1, (2012). "*Cement. composition, specifications and conformity criteria for common cements*." Warszawa: The Polish Committee for Standardization (Polski Komitet Normalizacyjny – PKN).

Pomaro, B., (2016). "A review on radiation damage in concrete for nuclear facilities: From experiments to modeling." *Modelling and Simulation in Engineering*, 2016, 4165746.

Pomaro, B., Gramegna, F., Cherubini, R., De Nadal, V., Salomoni, V. and Faleschini, F., (2019). "Gamma-ray shielding properties of heavyweight concrete with electric arc furnace slag as aggregate: an experimental and numerical study." *Construction and Building Materials*, 200, 188-197.

Reches, Y., (2019a). "A multi-scale review of the effects of gamma radiation on concrete." *Results in Materials*, 2, 100039.

Reches, Y., (2019b). "Quantification and modeling of the interactions of gamma radiation with concrete from bulk-scale observations." *International Journal of Concrete Structures and Materials*, 13(1), 59.

Richardson, I., Groves, G. and Wilding, C., (1989). "Effect of γ-radiation on the microstructure and microchemistry of GGBFS/OPC cement blends." *Mater. Res. Soc. Symp. Proc.*, 176, 31-37.

Rosseel, T. M., Maruyama, I., Le Pape, Y., Kontani, O., Giorla, A., Remec, I., Wall, J. J., Sircar, M., Andrade, C. and Ordonez, M., (2016). "Review of the current state of knowledge on the effects of radiation on concrete." *Journal of Advanced Concrete Technology*, 14(7), 368-383.

Saidani, K., Ajam, L. and Ouezdou, M. B., (2015) "Baryte powder as sand substitution in concrete: Effect on some mechanical properties." *Construction and Building Materials*, 95, 287-295.

Shariq, M., Prasad, J. and Abbas, H., (2013). "Effect of GGBFS on age dependent static modulus of elasticity of concrete." *Construction and Building Materials*, 41, 411-41.

Siddique, R. and Kaur, D., (2012). "Properties of concrete containing ground granulated blast furnace slag (GGBFS) at elevated temperatures." *Journal of Advanced Research*, 3(1), 45-51.

Vodak, F., Vydra, V., Trtik, K. and Kapickova, O., (2011). "Effect of gamma irradiation on properties of hardened cement paste." *Mater. Struct.*, 44, 101-107.

Wang, D., Shi, C., Farzadnia, N., Jia, H., Zeng, R., Wu, Y. and Lao, L., (2019). "A quantitative study on physical and chemical effects of limestone powder on properties of cement pastes." *Construction and Building Materials*, 204, 58-69.

Zhang, J., Bian, F., Zhang, Y., Fang, Z., Fu, C. and Guo, J., (2018). "Effect of pore structures on gas permeability and chloride diffusivity of concrete." *Construction and Building Materials*, 163, 402-413.